Damage Detection and Characterization in Composites Using a Geometric Modification of the RAPID Algorithm

Guillermo Azuara, Eduardo Barrera, Mariano Ruiz, and Dimitrios Bekas

***Abstract*—Structural Health Monitoring (SHM) of aircraft structures, which are manufactured more and more using composite material, is a well-established technique for increasing reliability and reducing maintenance costs. Implementing damage inspection algorithms that run in dedicated electronic systems helps reduce big data processing time with improved results. RAPID (Reconstruction Algorithm for Probabilistic Inspection of Damage) algorithm, developed some years ago, provides a technique to identify and characterize damages both in metallic and composite materials. However, this algorithm sometimes provides inaccurate predictions of the damage location, caused mainly by the influence of path intersection points among transducers, that can mask the current location of damages. This work presents a geometrical modification of standard RAPID algorithm (RAPID-G) that mitigates the influence of the intersection point between sensor paths. The results highlight that the location of damages improves significantly with this modification of the algorithm.**

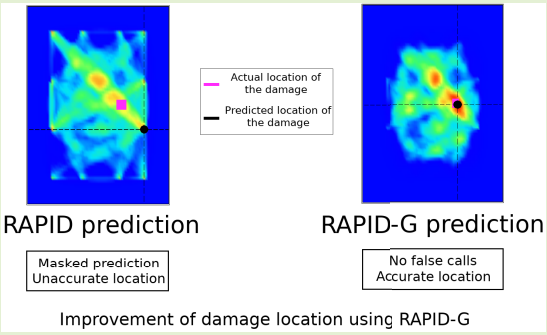

***Index Terms*— Structural health monitoring, composite, RAPID, Lamb waves, guided waves, damage detection, damage characterization.**

I. Introduction

STRUCTURAL Health Monitoring (SHM) systems integrate current non-destructive testing (NDT) techniques in structures, facilitating their status analysis and monitoring [1]. This implementation reduces maintenance costs and increases aeronautical structures' safety and reliability. This technology aims to achieve the highest level of automation for monitoring and providing data from structures in real-time. Lamb waves ultrasound testing [2] is one of the most widely used techniques for damage detection in aircraft structures. These waves (mechanical elastic) propagate through small thick material, while interacting with it and with damages that could exist within or on it. Lamb waves are generated via electrical excitation of piezoelectric transducers (PZT). These transducers can also be used to acquire signals propagating through structures. When performing these tests, it is advantageous to use embedded electronic systems, which can generate and acquire signals in multiple simultaneous channels, as well as process the acquired data [3]. In recent years, damage imaging methods, such as phased array imaging [4], [5] or delay-and-sum [6]–[8], have been widely used to detect damage position in plate-like structures in lamb wave-based SHM. However, these methods are not completely appropriate for composite material analysis, due to their usual anisotropy in terms of wave's group velocity. Therefore, we used the RAPID (Reconstruction Algorithm for Probabilistic Inspection of Damage) [9], [10] algorithm in this study. This algorithm is based on the comparison between the obtained signals in a transmitter-receiver transducers pair and a damage probability distribution. The geometry of the specimens and the transducer's distribution make RAPID algorithm very suitable to its utilisation [11]. In addition, the use of the standard algorithm on composites is very extended [12]–[14], as well as including modifications on the standard algorithm's parameters to improve its effectiveness [15]. This algorithm assigns an elliptical geometrical value to each direct path between

Manuscript received September 17, 2019; accepted October 24, 2019. Date of publication October 31, 2019; date of current version January 24, 2020. This work was supported in part by the European JTI-CleanSky2 Program under Grant 314768 (SHERLOC) and in part by the Regional Ministry of Education, Youth, and Sports of the Community of Madrid. The work of G. Azuara was supported by the European Social Fund under Grant PEJD-2016/TIC-3271. The associate editor coordinating the review of this article and approving it for publication was Prof. Guiyun Tian. *(Corresponding author: Eduardo Barrera.)*

G. Azuara, E. Barrera, and M. Ruiz are with the Instrumentation and Applied Acoustics Research Group, Universidad Politécnica de Madrid, 28031 Madrid, Spain (e-mail: g.azuara@upm.es; eduardo.barrera@upm.es; mariano.ruiz@upm.es).

D. Bekas is with the Structural Integrity and Health Monitoring Group, Department of Aeronautics, Imperial College London, London SW7 2AZ, U.K. (e-mail: d.bekas@imperial.ac.uk).

Digital Object Identifier 10.1109/JSEN.2019.2950748

transducers, resulting in an overlap between different ellipses, assigning higher values to points with more path intersections. To avoid this effect, we proposed a geometrical correction for the algorithm, based on the modification of the damage index of each point of analysis, in relation to its distance to each intersection point between paths.

The paper is divided into the following sections: In section II the materials and the set-up used for the experiment and the previous characterisation of the analysed materials are described. Sections III and IV provides the description of the standard version of RAPID algorithm, and the results obtained in the laboratory tests for damage detection in composite materials. Section V describes the main points of the proposal for the improvement of standard rapid algorithm (RAPID-G: geometrically modified RAPID), and the new results using this improved algorithm. Section VI provides the discussion of the obtained results, and finally Section VII offer the conclusions that have been reached after the completion of this work.

II. Materials

A. Experimental Set-Up

The system used for performing the experiments consisted of: a) a host computer where the user can configure the test parameters and receive the results (in this case a 2D image of the current state of the structure); b) an electronic embedded device connected to the host computer, which is capable of generating excitation signals, as well as acquiring and processing the resulting data; and c) surface-mounted PZT sensors on the structure's surface, connected to multiple channels of the embedded electronic device (Fig. 1; location of PZTs used). To get the dataset, some round-robin tests were performed, which consists of make simple tests (generating a sinusoidal burst applied to a PZT, and acquiring the signals received by the rest of PZT sensors) consecutively in all available channels, alternately changing the excitation channel between the available transducers [16].

Plates used in the tests are depicted in Fig. 1, and materials' characteristics are described in Table I. Twelve and eight PZTs were attached to the surface of thermoplastic-based (TP) and thermoset (TS) composites, respectively. PZT are DuraAct transducers with active disc D10 mm x TH 0.2 mm, from PiCeramic [17], bonded to the surface with an epoxy adhesive from DELO (AD821).

B. Specimens' Characterisation

1) Materials' Wave Propagation Characteristics: Materials' Lamb waves propagation characteristics depend on the group velocity for every path direction, both for the thermoplastic and thermoset composites. To calculate the propagation velocity of the Lamb wave, every path between transducers was checked, generating a signal from every transducer, which were acquired in the same way, obtaining for each direction of propagation a velocity value [18]. The group velocity diagram obtained for each material is depicted in Fig. 2.

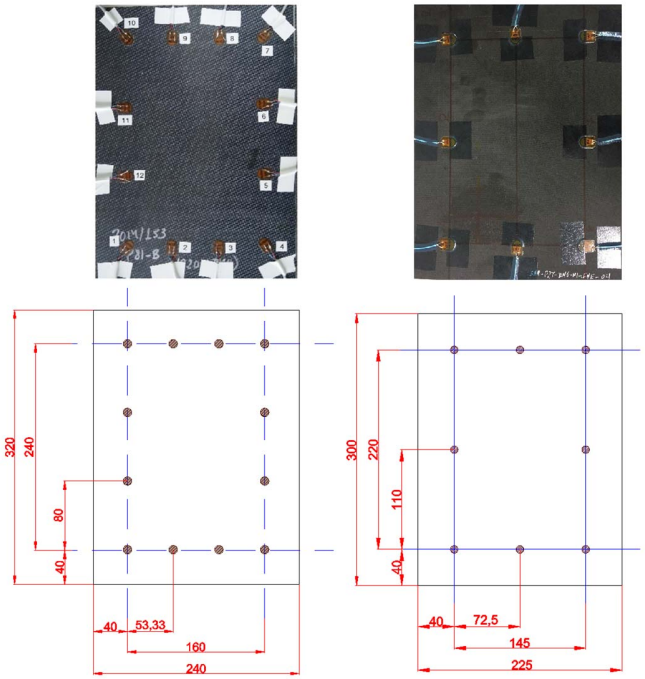

Fig. 1. (a) Thermoplastic matrix specimen; and (b) thermoset matrix composite material, with their dimensions (units in mm).

TABLE I
Materials' Characteristics

Matrix	Matrix polymer / Carbon fibre	Layers	Ply / Total thickness (mm)	Stacking Sequence
TP	Tenax-E TPCL PEEK-HTA40/ Tenax -E HTA40 3K	9	0.31 / 2.79	[0/90/+45/ -45/0/90/+45/-45/0]
TS	M21/194/34% /T800S Unidirectional Prepreg (Hexcel)/ Toray T800S	12	0.184 / 2.208	$[+45/-45/0_2/90/0]_S$

These results showed that the thermoplastic composite was almost isotropic in terms of group velocity, due to the similar values in every direction (a), while the thermoset matrix composite exhibited an anisotropic behaviour (b).

2) Signal Acquisition for Pristine State Material: Signal acquisition from pristine state materials was necessary for signal comparative analysis with damaged state materials. Signal generation and acquisition were performed using a round-robin test, which involved consecutively executing simple tests in all available channels, alternating excitation channels among the available transducers, starting from the first one and shifting through the rest, while acquiring the received signals using all the other sensors.

The characterisation of each material under baseline conditions occurred by conducting a set of tests using different

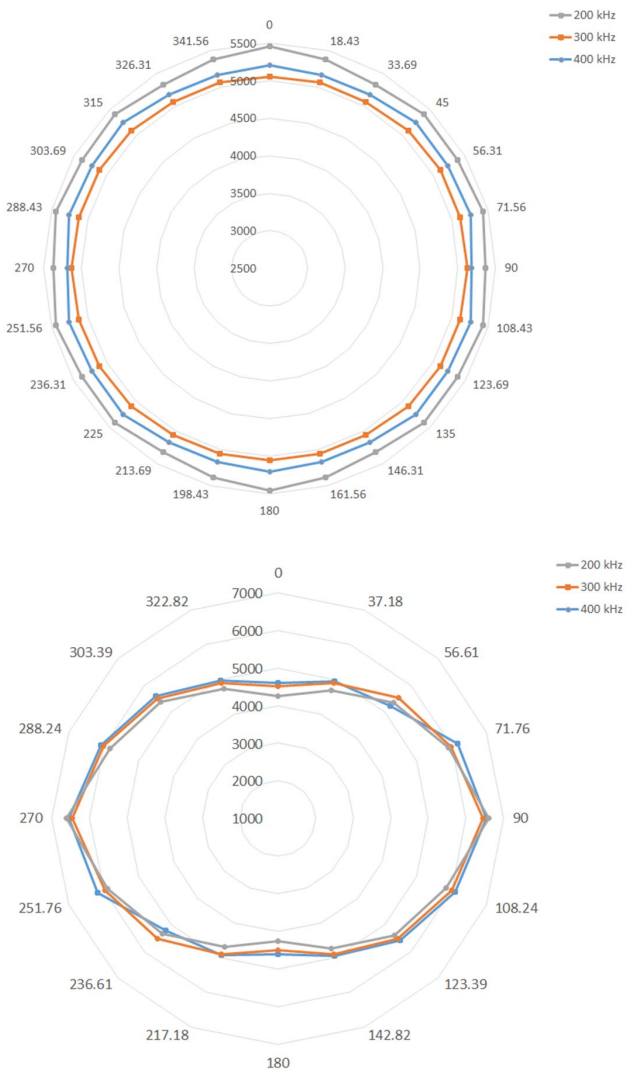

Fig. 2. Group velocity (m/s) obtained from the composite materials. (a) Thermoplastic matrix composite (quasi-isotropic). (b) Thermoset matrix composite (anisotropic).

frequency combinations, number of cycles, and windowing of excitation signals. For both composite materials, baseline characterization tests were carried out at ambient temperature and pressure conditions.

3) Damage Generation: Damage exerted on the thermoplastic matrix composite was simulated (using blu-tack) and, thereafter, performed using a visible shallow drill on the surface (0.8 mm depth and 7 mm diameter). Whereas, the thermoset composite was impacted using an Instron CEAST 9350 Drop Tower (Fig. 3). For the impact tests, a 20 J-energy impact event was performed using an impactor with a mass of 2.41 kg and 20 mm radius, resulting in a barely visible impact damage (BVID). The plate was supported in a fixture using a 200 mm $\times$ 200 mm window, and the impact test was performed at ambient temperature and pressure conditions. The main purpose of the impact tests was to create a BVID, and not to study the impact properties of composite materials.

Fig. 3. Instron CEAST 9350 drop tower impact system.

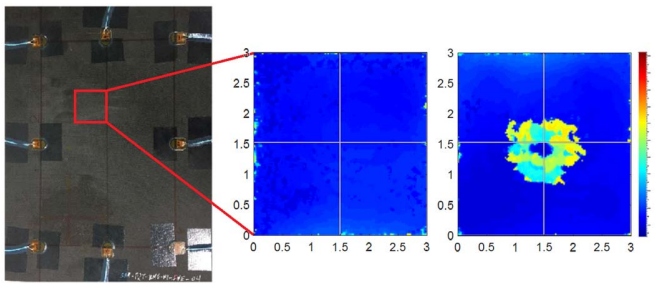

(a) (b) (c)

Fig. 4. (a) Analyzed area using C-Scan, with the impact point inside (x = 5.5 cm, and y = 14.5 cm). (b) C-Scan image of the pristine state. (c) C-Scan image after impact. All units in cm.

After the impact event, a C-Scan inspection was performed at the damage location area using a portable ultrasound camera system, DolphiCam supplied by DolphiTech, Norway. For the C-scan test, the sound velocity was set at 3070 m/s, and the inspection depth was at 2.79 mm (plate's thickness). The transmit/receive control and on-camera signal processing were performed by a Field Programmable Gate Array (FPGA). The excitation frequency was set at 3.8 MHz. An ultrasonic gel was employed as a coupling medium. To improve the analysis of the obtained images, a total number of eight was selected as a signal average. Initially, the received signals were amplified and filtered by an analog anti-aliasing filter with a cut-off frequency at 10 MHz. Afterwards, the acquired data were processed using the FPGA. At the end of the analysing process, the FPGA performed basic feature extraction on the signal indices. The studied quantity was time of flight, which, after the FPGA signal processing analysis, was displayed in a 2D graph at the DolphiCam software. Fig. 4 shows that the estimated damage area was approximately 132 mm^2. It should be mentioned the C-scan investigation was performed only in order to confirm the creation of the BVID.

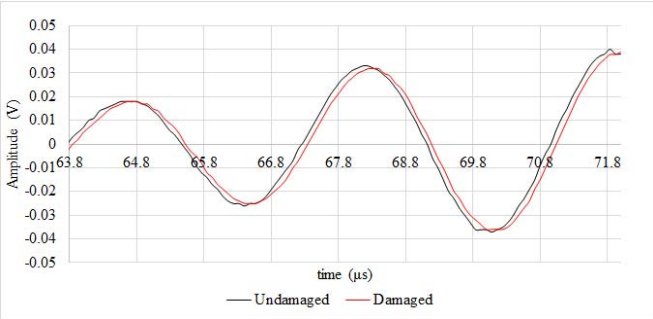

Fig. 5. Comparison between a signal of a specimen before and after damage induction.

III. Methods

This section introduces the method used initially for the damage detection in composite materials, the standard version of the RAPID algorithm.

The RAPID (Reconstruction Algorithm for Probabilistic Inspection of Defects) algorithm is a data processing algorithm proposed for damage detection in both metallic and composite structures [10]. The algorithm is based on two factors: the SDC (Signal Difference Coefficient), which indicates possible damage existing between a pair of transducers; and the elliptical spatial distribution E_{ij}, which assigns a value to each point of analysis according to its position with respect to the path on a pair of transducers. Two different mathematical methods have been used: the Correlation Coefficient Method (CCM) [10], and the Scaling Subtraction Method (SSM) [19], each has particular properties according to different types of signal variation [13], [14].

A. Correlation Coefficient Method

The SDC obtained using the Correlation Coefficient Method depends on the Pearson correlation coefficient ρ_{XY} between the signals [10]. This indicator is not too sensitive to a signal's amplitude linear variation, but is a good indicator of proportionality loss in amplitude, or a phase difference between both signals (Fig. 5). Furthermore, the correlation coefficient is sensitive to frequency changes or flight time variations [19].

B. Scaling Subtraction Method

In this case, SDC was obtained using the Scaling Subtraction Method (SSM). This value was obtained by calculating the area between signals from the integration of their squared-difference [19]. However, the lack of signal scalability due to amplitude differences in excitation or to the non-linearity of the material (which causes the acquired signals to be non-proportional) [20], made it necessary to previously scale the signals (Fig. 6). The loss of proportionality became evident, obtaining an indicator of damage according to the non-linearity of the material.

Once the previous values were determined, it was possible to obtain the SDC indicator, by integrating signal differences (Fig. 7). In addition to its sensibility to the material-related loss of proportionality, the SSM provided good results with changes in the amplitude (signal attenuation).

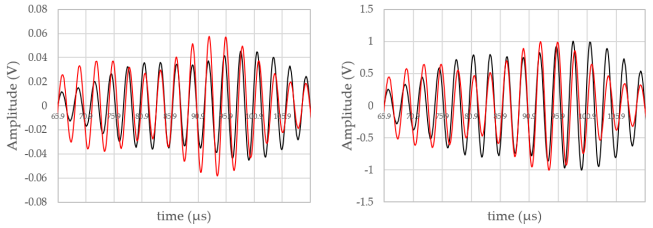

Fig. 6. (a) Signals without scaling. (b) Scaled signals; in red, high amplitude excitation signal (12 V_{PP}), and in black, low amplitude excitation signal (8 V_{PP}).

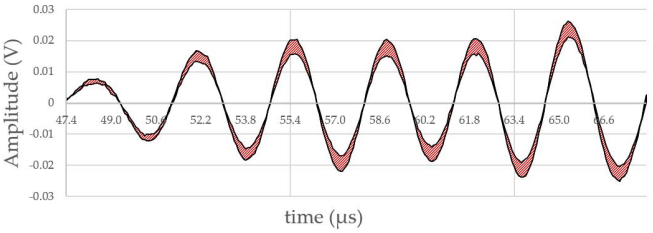

Fig. 7. The colored area is the difference calculated by the SSM method (n = 6 periods).

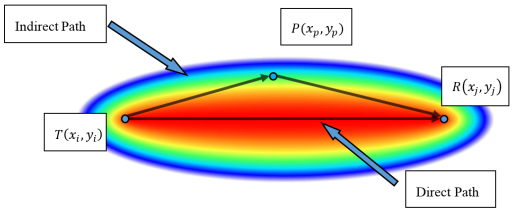

Fig. 8. Elliptical distribution of the RAPID algorithm.

C. Spatial Distribution and Damage Index Calculation

The spatial distribution (elliptical and linearly decreasing from the direct path, placing the transducers in the foci) considers that the probability of a defect causing signal alteration is greater the closer it is to the direct path between a pair of transducers (Fig. 8) [16].

The following equations (1) (2) (3) [10] rule the spatial distribution, for the point of analysis $P(x_p, y_p)$ and the transmitter i and receiver j:

$$E_{ij}\left(x_p, y_p\right) = \left[\frac{\beta - R_{ij}\left(x_p, y_p\right)}{\beta - 1}\right] \tag{1}$$

$$R_{ij}\left(x_p, y_p\right) = \begin{cases} RD_{ij}(x_p, y_p) if\, RD_{ij}(x_p, y_p) < \beta \\ 0\ if\, RD_{ij}(x_p, y_p) \geq \beta \end{cases} \tag{2}$$

$$RD_{ij}\left(x_p, y_p\right) = \frac{\sqrt{(x_p - x_i)^2 + (y_p - y_i)^2} + \sqrt{(x_p - x_j)^2 + (y_p - y_j)^2}}{\sqrt{(x_j - x_i)^2 + (y_j - y_i)^2}} \tag{3}$$

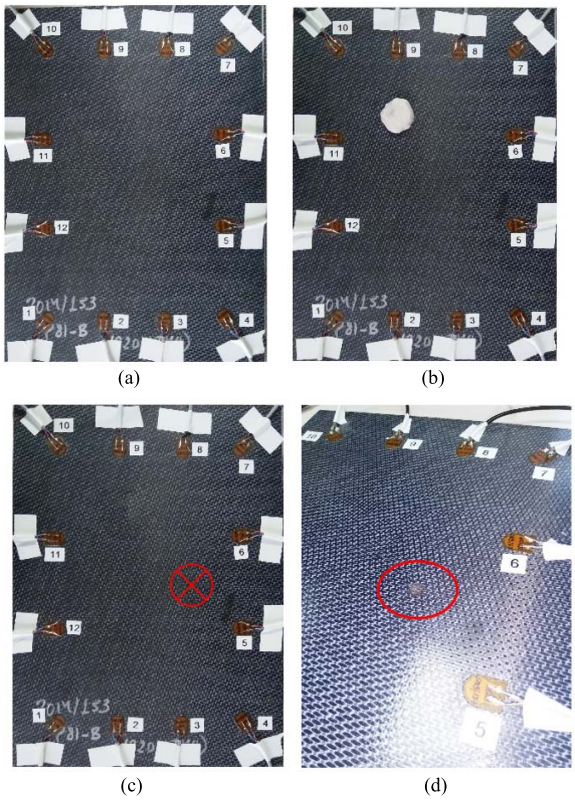

Fig. 9. (a) Pristine state of the thermoplastic plate (transducer 1 is [x = 0, y = 0]). (b) Simulated damage [x = 6.0 cm, y = 17.0 cm]. (c) Real damage [x = 11.5 cm, y = 12.0 cm]. (d) Detail of the shallow drill (real damage).

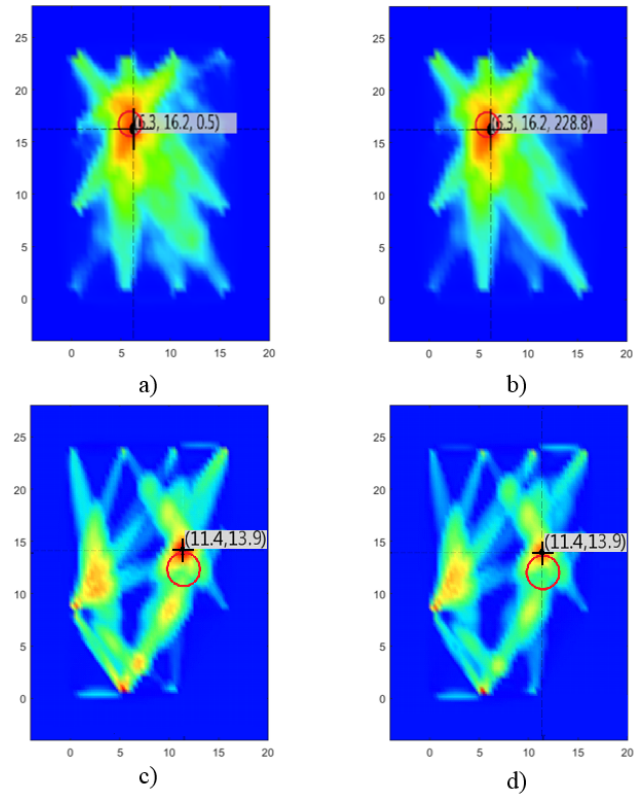

Fig. 10. Results using: (a) CCM indicator; (b) SSM indicator, for simulated damage; (c) CCM indicator; and (d) SSM indicator, for real damage (units in cm). Red circles indicate the actual location of the damage, and black cross points indicated the predicted location of the damage using the standard RAPID algorithm.

where:

- E_{ij}: is the value of the elliptical distribution in the point of analysis $P(x_p, y_p)$.
- β: is the value which limits the size of the ellipse, through the factor R_{ij}.
- RD_{ij}: is the ratio between the distance of the indirect path and direct path.

Finally, by combining SDC values using CCM or SSM, the sum of all signal contributions at the point to be analysed (damage index) was calculated as follows:

$$P(x_p, y_p) = \sum_{i=1}^{N} \sum_{j=1, j\neq i}^{N} SDC_{ij} E_{ij} \left(x_p, y_p\right) \tag{4}$$

IV. Results

The following paragraphs contain the results obtained from the processed signals using standard RAPID algorithm.

A. Tests Using Data Comparison From the Structure's Pristine State

Damage detection in this type of tests is possible by comparing information from the structure's previous state (pristine state) to the current state. Thus, the damage can be detected using any of the two methods for estimating the SDC.

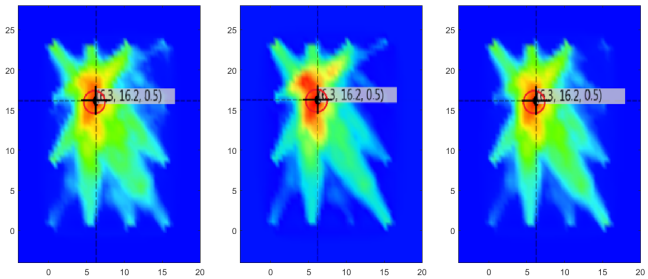

Fig. 11. Results depending on the frequency of excitation, using SSM indicator for the simulated damage. (a) 250 kHz. (b) 300 kHz. (c) 350 kHz (position units in cm).

1) Thermoplastic Matrix Specimen: The thermoplastic material specimen (using blu-tack in order to simulate a damage, and then drilling the plate's surface) is depicted in Fig. 9. The excitation signal was a sine wave of 1.5 cycles, with 12 V_{PP} (Volts peak-to-peak) amplitude, and 380 kHz frequency. In order to obtain the results, previously acquired information from the pristine state (at same conditions of excitation) was compared to that from the damaged situation, using the standard RAPID algorithm.

Fig. 10 depicts the results from the thermoplastic matrix specimen, which were obtained using both CCM and SSM indicators. The images show that the damage was located in an accurate location. This method is very robust and adaptable to changes in excitation frequency (Fig. 11).

TABLE II
ABSOLUTE ERROR (mm)

Type of damage	ε_x	ε_x	Total distance
Simulated (CCM)	3	8	8.5
Simulated (SSM)	3	8	8.5
Real (CCM)	1	19	19.1
Real (SSM)	1	19	19.1

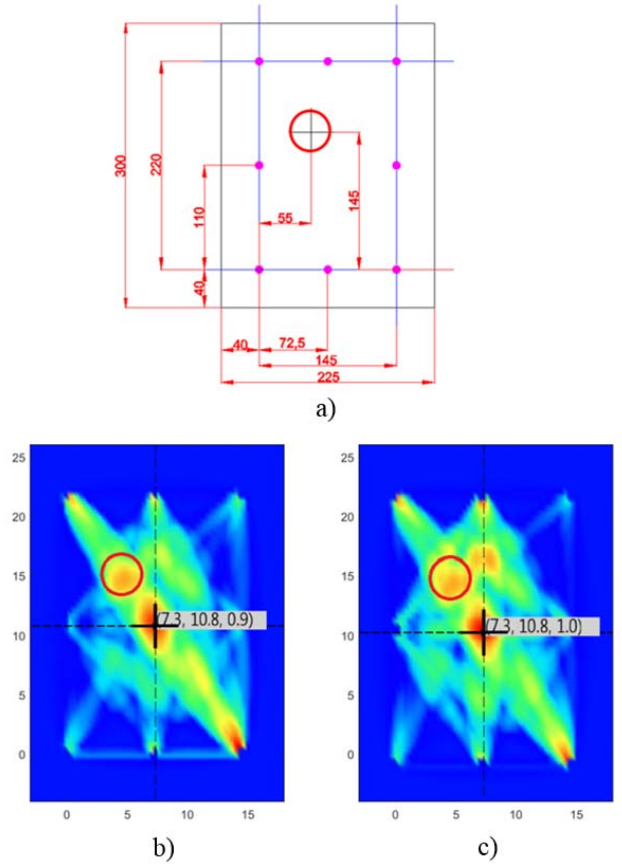

Fig. 12. (a) Impact location in thermoset specimen [x = 5.5 cm, y = 14.5 cm]. (b) Predicted damage location using 1.5 cycles. (c) Predicted damage location using 4.5 cycles. Red circles indicate the actual location of the damage, and black cross points indicate the predicted location of the damage using the standard RAPID algorithm.

The accuracy of the damage location using this method was high. The absolute error for each result (Total distance = ‖ real position – predicted position ‖ = $\sqrt{\varepsilon_x^2 + \varepsilon_y^2}$) is summarized in Table II.

2) Thermoset Matrix Specimen: After impact, thermoset specimen tests were performed at controlled room temperature. The tests were carried out at the same conditions of excitation as those of the baseline tests. The impact and predicted damage locations in the thermoset specimen are depicted in Fig. 12.

The obtained deviation from the actual damage location, calculated in Table III, was very high, which was due to the higher damage index values obtained in some specific positions in the analysed area, thus causing an erroneous prediction of the damage location.

TABLE III
ABSOLUTE ERROR (mm)

Number of cycles	ε_x	ε_x	Total distance
1.5	18	37	41.1
4.5	18	37	41.1

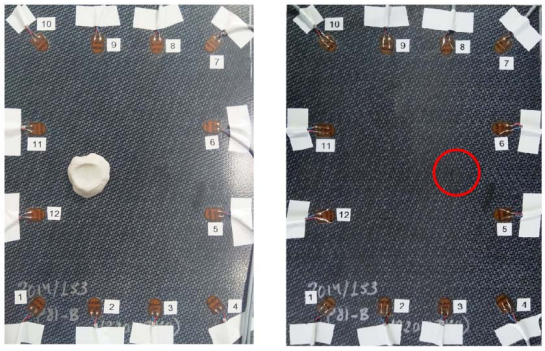

Fig. 13. (a) Simulated damage [x = 5.3 cm, y = 12.0 cm]. (b) Real damage [x = 11.5 cm, y = 12.0 cm].

TABLE IV
ABSOLUTE ERROR (mm)

Type of damage	ε_x	ε_x	Total distance
Simulated (SSM)	1	3	3.2
Real (SSM)	12	3	12.4

B. Tests Using Data Only From the Structure's Current State

The previous section presented results using information from the structure's pristine state. However, it is possible to detect and locate damages in the structure even without this information. In this context, and to avoid the lack of the structure's previous information, the system performed two tests with different signal excitation amplitude values (high level and low level), thereby obtaining two different sets of data as inputs for the RAPID algorithm.

1) Thermoplastic Matrix Specimen: Fig. 13 depicts thermoplastic material specimens, using both simulated and real damage. Two tests were conducted for damage detection, using V_{high} = 12 V_{PP} and V_{low} = 8 V_{PP}, 35 cycles of excitation, Hanning windowing, and a frequency of 380 kHz, at room temperature (25 $^{\circ}C \pm 2\ ^{\circ}C$). The results are depicted in Fig. 14, showing an accurate location of the damage. These results were processed using the SSM indicator, due to the lack of material scalability when using different amplitude levels, rendering the CCM indicator inefficient.

The images show that the results were very accurate. The absolute error value for each axis, as well as the total distance from the predicted damage to the actual one, are summarised in Table IV.

2) Thermoset Matrix Specimen: Similarly, thermoset specimen tests were carried out using V_{high} = 12 V_{PP} and V_{low} = 8 V_{PP} signals, 35 excitation cycles, Hanning windowing, and

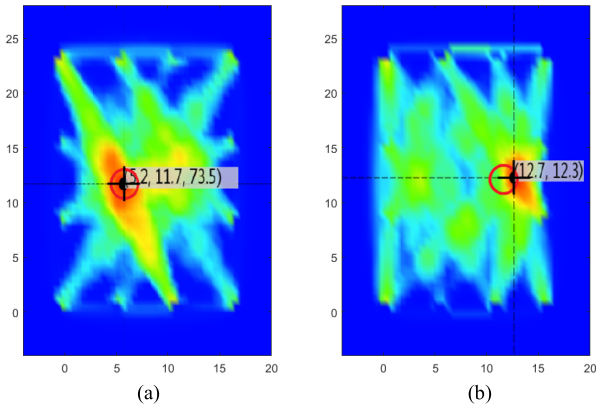

Fig. 14. Predicted damage location for the simulated (a) and real (b) damage. Red circle indicates the actual location of the damage, and black cross points to the predicted location of the damage.

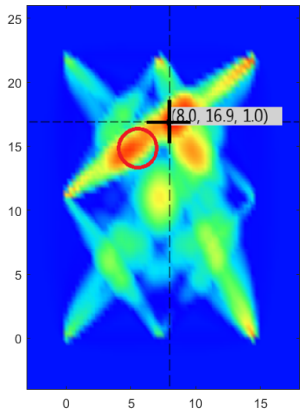

Fig. 15. Results from the impacted thermoset matrix composite specimen. Red circle indicates the actual location of the damage, and black cross points to the predicted location of the damage.

TABLE V
ABSOLUTE ERROR (mm)

Frequency	ε_x	ε_x	Total distance
350 kHz	25	24	34.6

350 kHz frequency, on the impacted plate. Fig. 15 depicts the obtained results.

The image shows that in this case the results are not accurate. The absolute error value for each axis and the total distance from the predicted damage to the actual one are summarized in Table V.

These results, as well as those previously obtained using the pristine state information, were not appropriate.

Assuming the thermoset specimen results were inaccurate due to geometrical masking, we propose an algorithm modification in the following section.

V. PROPOSAL FOR THE IMPROVEMENT OF STANDARD RAPID ALGORITHM. RAPID-G: GEOMETRICALLY MODIFIED RAPID

The RAPID algorithm, in its geometrical term, assigns a bigger value as the number of a path's intersection points between transducers increases (Fig. 16). In the area near the intersection point between paths, the sum of the damage index is higher, especially at the exact point.

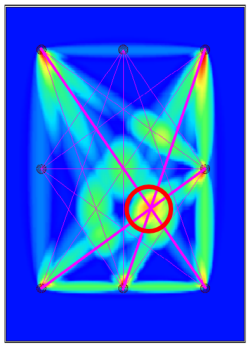

Fig. 16. Thermoset matrix composite plate. All paths, crossing in 29 points inside the area where the transducers delineate, are represented. The selected paths, highlighted in bold, intersect at the point marked by the red circle.

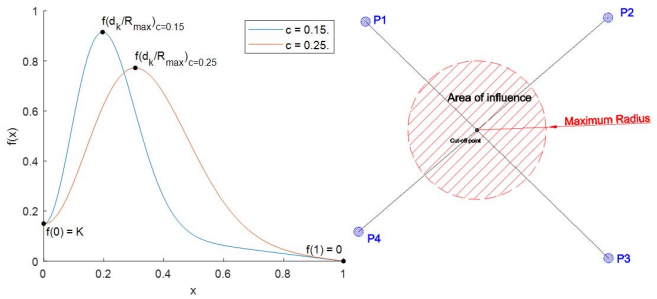

Fig. 17. Shape function (a) for two values of c. The proposed function sets a zero slope on the initial point (the intersection point between paths), and assigns a zero value to the points located beyond the maximum relative radius (b).

The results obtained from the thermoset matrix specimen showed inaccurate results, using both baseline pristine and baseline-free processing. To improve the algorithm, and to decrease the effect of masking, a geometrical modification was proposed (RAPID-G).

A. RAPID-G Proposal

To avoid the effect of geometrical masking, the shape function (5) has been proposed, which consists of a negative exponential function, a quadratic function (which places in the intersection point a zero slope), and a decreasing linear function (Fig. 17). The K factor is the vertical axis-intercept, and the c factor controls the width (or the standard deviation) of the exponential function:

$$f(x) = \left(\frac{e}{2c^2} \cdot e^{-\frac{x^2}{2c^2}} \cdot x^2 + K \right) \cdot (1 - x) \tag{5}$$

This function is located with its origin in the previously calculated intersection point of two or more paths between transducers, and its influence reaches a maximum point of analysis located at a maximum radius defined by the user, which establishes the correction's area of influence.

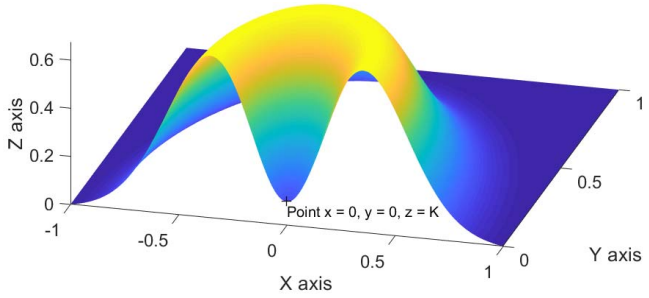

Fig. 18. Development of the shape function around the vertical axis placed on the intersection point. The figure shows half surface; the whole surface is XZ-plane symmetric.

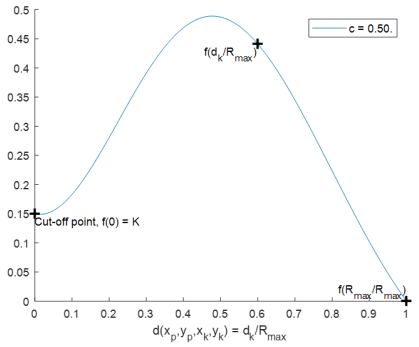

Fig. 19. Shape function used for the correction of all tests in RAPID-G.

A weight factor for each intersection point is added to the modification, due to the different number of paths which concur at the same point, increasing the final value of the damage index as the number of paths which cross that point increases.

This modification is applied to each point of analysis, rendering the sum of all correction values at each intersection between paths within the area of influence. The resulting (6) is the combination of (4) and (5):

$$P\left(x_p, y_p\right) = \sum_{i=1}^{N} \sum_{j=1, j\neq i}^{N} \left[SDC_{ij} \left[\frac{\beta - R_{ij}\left(x_p, y_p\right)}{\beta - 1} \right] \right] \cdot \sum_{k=1}^{M} \left[\left(\frac{e}{2c^2} \cdot e^{-\frac{d_k^2}{2c^2}} \cdot d_k^2 + K \right) \cdot (1 - d_k) \cdot w_k \right] \quad (6)$$

where:

M: number of intersection points inside the analysed area;

$\frac{e}{2c^2}$: this term normalizes the exponential function;

c: width parameter of the exponential function;

K: z-intercept of the correction function;

w_k: weight factor, which depends on the number of paths which cut the intersection point k; and

d_k: relative distance from the junction point (x_k, y_k) to the point of analysis (x_p, y_p):

$$d(x_p, y_p, x_k, y_k) = \sqrt{\left(x_p - x_k\right)^2 + \left(y_p - y_k\right)^2} \quad (7)$$

$$d_k(x_k, y_k) = \begin{cases} \dfrac{d\left(x_p, y_p, x_k, y_k\right)}{R_{max}} & if\ d \leq R_{max} \\ 1 & if\ d > R_{max} \end{cases} \quad (8)$$

The development of the function around a vertical axis placed in the junction point is the modification for a single intersection point (Fig. 18), symmetric on the y-axis. The total sum of these modifications alters the final value of the damage index.

B. Results Using RAPID-G Algorithm

Baseline comparison and baseline-free tests have been carried out to detect damages in the thermoset matrix composite specimen using the modified algorithm RAPID-G.

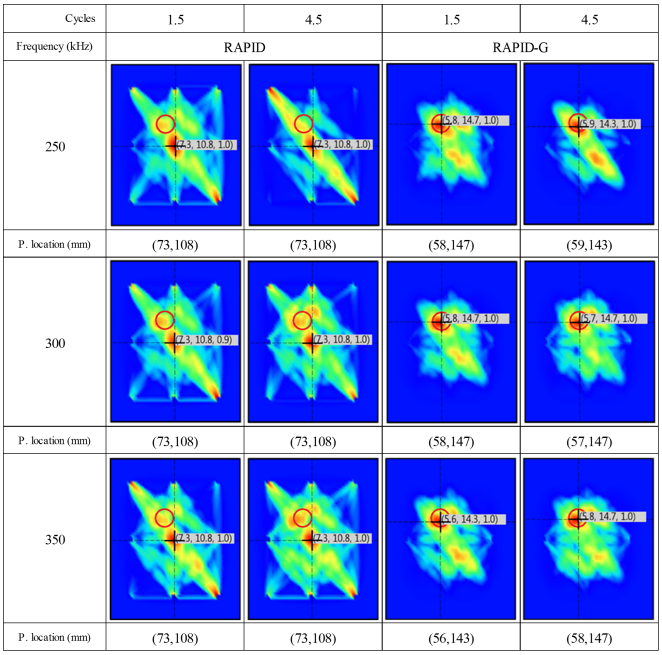

Fig. 20. Predicted location of the damage after signal processing using baseline information. Results using the standard RAPID algorithm (left). Results from the same signals using RAPID-G (right). Red circles point to the actual damage [x = 5.5 cm, y = 14.5 cm], and black crosses point to the predicted location of the damage.

1) Tests Using Data Comparison From the Pristine State of the Structure: The standard RAPID algorithm we performed did not provide an accurate damage position in the impacted thermoset coupon, because it was masked by higher damage index values primarily located at the distribution's central point, where the number of paths crossing this point was the highest (four direct paths).

To avoid this effect, the proposed modification of RAPID (RAPID-G) was applied. The selected parameters used on the shape function were K = 0.15, R_{max} = 0.05 m, and c = 0.50 (Fig. 19). These parameters were adjusted during signal processing to obtain the best detection performance.

Using RAPID-G, the obtained results for baseline comparison are depicted in Fig. 20 (a comparison between previous results and improved results).

The absolute error is calculated in Table VI, using the distance from the actual damage location (x = 5.5 cm, y = 14.5 cm) to the predicted location of the damage.

TABLE VI
ABSOLUTE ERROR (mm)

Frequency (kHz)	Standard RAPID		RAPID-G	
Cycles	1.5	4.5	1.5	4.5
250	41.1	41.1	3.6	4.5
300	41.1	41.1	3.4	2.8
350	41.1	41.1	2.2	3.6

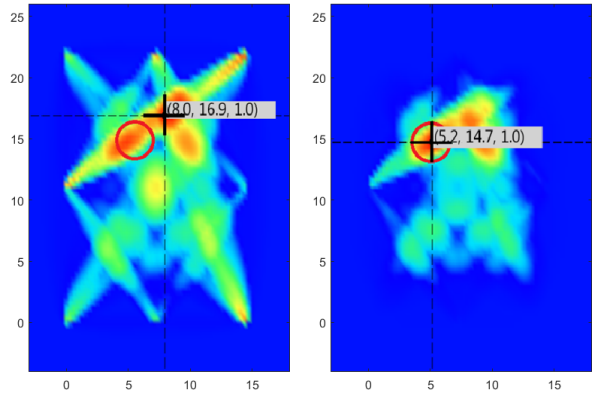

Fig. 21. Predicted location of the damage using current state information. (a) Results using standard RAPID. (b) Results using RAPID-G. The red circles point to the actual damage [x = 55.0, y = 145.0], and black crosses point to the predicted damage.

TABLE VII
ABSOLUTE ERROR (mm)

Frequency (kHz)	Standard RAPID	RAPID-G
350	34.6	3.6

The RAPID-G algorithm provides an accurate damage location prediction in all analysed cases.

2) Tests Using Data Only From the Current State of the Structure: Comparative tests used the following signal characteristics: $V_{high} = 12\ V_{PP}$ and $V_{low} = 8\ V_{PP}$, 35 excitation cycles, Hanning windowing, and a frequency of 350 kHz, carried out on the impacted thermoset plate. In addition to the tests performed using baseline information, images obtained using the standard RAPID method showed masked results.

The shape function modified RAPID algorithm on these tests was the same as the previous section ($K = 0.15$, $R_{max} = 0.05$ m, and $c = 0.50$; Fig. 19). Previous tests on the thermoset matrix specimen gave an inaccurate prediction (Fig. 15).

Fig. 21 shows results of the baseline-free method, using both standard RAPID and improved RAPID-G. The error was calculated from the position of the predicted damage to the position of the actual damage (Table VII). The RAPID-G algorithm provided an accurate prediction of the damage location.

VI. DISCUSSION

Damage detection and localization using standard RAPID in thermoplastic matrix specimens show accurate results with respect to the actual location, and compared to the pristine state information (Table II, absolute error ∼20 mm) or using only the current state information (Table IV, <15 mm). However, the results in the thermoset specimen are not good (Table III; for baseline test and Table V for baseline-free test, >35 mm). In addition, the maximum value point is always located in a path intersection point between transducers (Fig. 12, for the baseline test located at the central point; and Fig. 15, for current situation test).

These experimental results led the authors of this work to suspect the negative influence on the damage location caused by the increase in damage index at the intersection points between transducers. Based on this fact, a geometric modification of the standard RAPID algorithm was proposed and developed. The main goal of this improvement was to try to counteract the negative effect mentioned above.

The use of the RAPID-G algorithm in thermostable specimens demonstrates that the location of the damage can be improved with the geometric modification proposed. In Table VI, the absolute error for the baseline test changed from >40 mm to <5 mm and, in Table VII, the error changed from 35 mm to 4 mm for the baseline free test.

VII. CONCLUSIONS

Damage detection and localization in composite materials using the standard RAPID algorithm is only possible under specific circumstances. The algorithm calculates the damage index between two signals from two different states, obtained through the SDC (Signal Difference Coefficient). The Correlation Coefficient Method (CCM) and the Scaling Subtraction Method (SSM) can be used to detect and locate damages using data comparison to the pristine state of the structure, while only the Scaling Subtraction Method (SSM) is suitable for characterising damages using data only from the current state of the structure.

However, some types of damage are masked by high damage index values caused by geometrical characteristics of the standard RAPID algorithm.

RAPID-G, the proposed geometrical modification for the RAPID algorithm described in this paper, avoids this problem. This modification allows unmasking of slight damages, in which damage indexes would be lower than the assigned value to the intersection points by the standard algorithm. This modification provides good results, using baseline information as well as only current situation data. The results obtained show that the accuracy of the location increases considerably using RAPID-G, in most cases with an accuracy in the order of half-centimetre with respect to the actual damage. In this study, RAPID-G was tested in composite plates, but in the future we aim to test it in bigger and more complex components and also in metallic structures. This new algorithm, combined with some type of electronic embedded system, as described in [3], and using an analysis methodology [21], could provide a promising platform for applying SHM technologies in this field [22].

ACKNOWLEDGMENT

The authors would like to thank the FIDAMC for providing the thermoplastic material.

REFERENCES

[1] D. Balageas, C. P. Fritzen, and A. Güemes, Eds., *Structural Health Monitoring*, vol. 90. Hoboken, NJ, USA: Wiley, 2010.

[2] V. Giurgiutiu, "Lamb wave generation with piezoelectric wafer active sensors for structural health monitoring," *Proc. SPIE*, vol. 5056, pp. 111–123, Aug. 2003.

[3] G. Aranguren, P. M. Monje, V. Cokonaj, E. Barrera, and M. Ruiz, "Ultrasonic wave-based structural health monitoring embedded instrument," *Rev. Sci. Instrum.*, vol. 84, no. 12, 2013, Art. no. 125106.

[4] K. R. Leonard, E. V. Malyarenko, and M. K. Hinders, "Ultrasonic Lamb wave tomography," *Inverse Problems*, vol. 18, no. 6, p. 1795, 2002.

[5] P. Malinowski, T. Wandowski, I. Trendafilova, and W. Ostachowicz, "A phased array-based method for damage detection and localization in thin plates," *Struct. Health Monit.*, vol. 8, pp. 5–15, Apr. 2009.

[6] J. E. Michaels, "Detection, localization and characterization of damage in plates with an *in situ* array of spatially distributed ultrasonic sensors," *Smart Mater. Struct.*, vol. 17, May 2008, Art. no. 035035.

[7] C. H. Wang, J. T. Rose, and F.-K. Chang, "A synthetic time-reversal imaging method for structural health monitoring," *Smart Mater. Struct.*, vol. 13, no. 2, p. 415, 2004.

[8] Z. Sharif-Khodaei and M. H. Aliabadi, "Assessment of delay-and-sum algorithms for damage detection in aluminium and composite plates," *Smart Mater. Struct.*, vol. 23, no. 7, May 2014, Art. no. 075007.

[9] T. Hay, R. Royer, H. Gao, X. Zhao, and J. Rose, "A comparison of embedded sensor Lamb wave ultrasonic tomography approaches for material loss detection," *Smart Mater. Struct.*, vol. 15, no. 4, p. 946, 2006.

[10] X. Zhao *et al.*, "Active health monitoring of an aircraft wing with embedded piezoelectric sensor/actuator network: I. Defect detection, localization and growth monitoring," *Smart Mater. Struct.*, vol. 16, p. 1208. Jun. 2007.

[11] F. Lambinet *et al.*, "Effectiveness of RAPID and SSM algorithms on composite scarf repair," *Key Eng. Mater.*, vol. 774, pp. 535–540, Aug. 2018.

[12] M. Tabatabaeipour, J. Hettler, S. Delrue, and K. Van Den Abeele, "Reconstruction algorithm for probabilistic inspection of damage (RAPID) in composites," in *Proc. 11th Eur. Conf. Non-Destructive Test. (ECNDT)*, Oct. 2014, pp. 1–8.

[13] M. Dziendzikowski, A. Kurnyta, K. Dragan, S. Klysz, and A. Leski, "*In situ* Barely Visible Impact Damage detection and localization for composite structures using surface mounted and embedded PZT transducers: A comparative study," *Mech. Syst. Signal Process.*, vol. 78, pp. 91–106. Oct. 2016.

[14] B. Yang, F.-Z. Xuan, S. Chen, S. Zhou, Y. Gao, and B. Xiao, "Damage localization and identification in WGF/epoxy composite laminates by using Lamb waves: Experiment and simulation," *Compos. Struct.*, vol. 165, pp. 138–147. Apr. 2017.

[15] Z. Liu, X. Zhong, T. Dong, C. He, and B. Wu, "Delamination detection in composite plates by synthesizing time-reversed Lamb waves and a modified damage imaging algorithm based on RAPID," *Struct. Control Health Monit.*, vol. 24, no. 5, p. e1919, 2017.

[16] G. Azuara, E. Barrera, and M. Ruiz, "Integration of algorithms for damage detection in thermoplastic materials inside electronic embedded devices," in *Proc. Eur. Workshop Struct. Health Monit. Ser. (EWSHM)*, 2018, pp. 1–12.

[17] (Aug. 2003). *PiCeramic Piezoelectric Actuators Datasheet*. [Online]. Available: https://static.piceramic.com/fileadmin/user_upload/physik_instrumente/files/CAT/PI_CAT128E_R3_Piezoelectric_Actuators.pdf?_ga=2.137927666.39786750.1550763551-149680812.1550763551

[18] Z. Lašová and R. Zemcík, "Determination of group velocity of propagation of Lamb waves in aluminium plate using piezoelectric transducers," *Appl. Comput. Mech.*, vol. 11, no. 1, pp. 23–32, 2017.

[19] M. Tabatabaeipour, J. Hettler, S. Delrue, and K. Van Den Abeele, "Visualization of delaminations in composite structures using a baseline-free, sparse array imaging technique based on nonlinear Lamb wave propagation," *Acta Acustica United With Acustica*, vol. 103, pp. 987–997, Dec. 2017, doi: 10.3813/AAA.919128.

[20] M. Scalerandi, "Power laws and elastic nonlinearity in materials with complex microstructure," *Phys. Lett. A*, vol. 380, no. 3, pp. 413–421, 2016.

[21] Z. S. Khodaei and M. H. Aliabadi, "A multi-level decision fusion strategy for condition based maintenance of composite structures,"*Materials*, vol. 9, no. 9, p. 790, 2016, Sep. 2016.

[22] S. Beard, B. Liu, P. Qing, and D. Zhang, "Challenges in implementation of SHM," in *Proc. 6th Int. Workshop Struct. Health Monit.*, Stanford, CA, USA, Stanford University, Sep. 2007, pp. 11–13.

Guillermo Azuara was born in Madrid, Spain, in 1990. He received the M.Sc. degree in mechanical and industrial engineering from Universidad Politécnica de Madrid, Spain, in 2016, where he joined the Ph.D. degree in 2017.

He is currently with the Instrumentation and Applied Acoustics Research Group, Universidad Politécnica de Madrid. His current research interests include Lamb waves-based structural health monitoring (SHM) and the development of electronic devices for signal generation, acquisition, and processing, applied to aircraft structures.

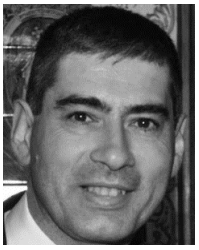

Eduardo Barrera was born in Vitoria, Spain, in 1968. He received the M.Sc. degree in telecommunication engineering and the Ph.D. degree from Universidad Politécnica de Madrid, Spain, in 1993 and 2008, respectively.

He was an Invited Researcher with Imperial College London in 2017. He is currently a Full Professor with the Department of Electronic Engineering and Computer Science. He is the Leader of the structural health monitoring (SHM) research area with the Instrumentation and Applied Acoustics Research Group, Universidad Politécnica de Madrid. He is the coauthor of more than 50 articles in peer-reviewed journals. His current research interest includes the development of electronic devices and data processing algorithms for damage detection and characterization related to structural health monitoring in aeronautics based on Lamb waves.

Dr. Barrera won the Best Practical SHM Solution Award from Airbus at the European Workshop in SHM 2012. He received the Salvador de Madariaga Fund in 2017.

Mariano Ruiz was born in Madrid, Spain, in 1967. He received the B.S. and M.S. degrees in telecommunications engineering from Universidad Politécnica de Madrid, in 1989 and 1997, respectively, and the Ph.D. degree from Universidad Politécnica de Madrid, in 2002.

He was the Chair of instrumentation and embedded systems with Universidad Politécnica de Madrid, where he teaches courses on analog and digital electronics, microprocessors, DSPs, embedded systems, FPGA, SoCs, and instrumentation systems. He is with the Instrumentation and Applied Acoustics Research Group, Universidad Politécnica de Madrid, where he works in the fields of instrumentation and virtual instrumentation systems, with a special emphasis in research on data acquisition and real-time data processing architectures for big science experiments and fusion devices using FPGAs and GPUs. He is the author of more than 70 research articles. He has taken part in many research projects.

Dimitrios Bekas was born in Amyndeon, Greece, in 1988. He received the Diploma and M.Sc. degrees in materials science and engineering and the Ph.D. degree from the University of Ioannina, Greece, in 2015 and 2017, respectively.

He was an Invited Researcher with Chalmers University of Technology in 2016. Since 2017, he has been a Research Associate with the Structural Integrity and Health Monitoring Group, Department of Aeronautics of Imperial College London, U.K. He is the author of 16 research articles published in international scientific journals. He has presented his work in ten international conferences. His research interests include multifunctional composites, 3D printing technologies, self-sensing and self-healing composites, structural health monitoring technologies (impedance spectroscopy, acoustic emission, ultrasound, and guided waves), and carbon-modified polymer composites.

Dr. Bekas received the Rune Bernhardsson's Graphene Fund. He has also received the Outstanding Reviewer Award for the journal *Composites Part A: Applied Science and Manufacturing* (Elsevier) in 2017. He is a regular reviewer of five scientific journals.